Environmental Science & Technology

Article

Cite This: Environ. Sci. Technol. 2019, 53, 5212−5220

pubs.acs.org/est

Cationic Covalent Organic Nanosheets for Rapid and Selective Capture of Perrhenate: An Analogue of Radioactive Pertechnetate from Aqueous Solution

Hong-Ju Da,[†] Cheng-Xiong Yang,[†] and Xiu-Ping Yan*[,‡,§]

[†]Research Center for Analytical Sciences, Tianjin Key Laboratory of Molecular Recognition and Biosensing, College of Chemistry, Nankai University, Tianjin 300071, China

[‡]State Key Laboratory of Food Science and Technology, International Joint Laboratory on Food Safety, Institute of Analytical Food Safety, School of Food Science and Technology, Jiangnan University, Wuxi 214122, China

[§]Collaborative Innovation Center of Chemical Science and Engineering (Tianjin), Tianjin 300071, China

Supporting Information

ABSTRACT: Capture of radioactive TcO_4^- from nuclear wastes is extremely desirable for waste disposal and environmental restoration. Here, we report the synthesis of hydrolytically stable cationic covalent organic nanosheets (iCON) for efficient uptake of ReO_4^-, a nonradioactive surrogate of TcO_4^-. The iCON combines cationic guanidine-based knots with hydroxyl anchored neutral edge units and chloride ions loosely bonded in the pores, rendering extremely fast exchange kinetics toward ReO_4^- with high uptake capacity of 437 mg g^{-1} and prominent distribution coefficient of 5.0×10^5. The removal efficiency remains stable over a pH range of 3−12 and allows selective capture of ReO_4^- in the presence of excessive competing anions such as NO_3^-, CO_3^{2-}, PO_4^{3-} and SO_4^{2-} with good removal efficiency for ReO_4^- in a simulated Hanford LAW Melter Recycle Stream. Anion exchange between the ReO_4^- in solution and the chloride ion in iCON plays dominant role in the adsorption of ReO_4^-. The iCON shows promise for effective removal of radioactive ^{99}Tc from nuclear waste.

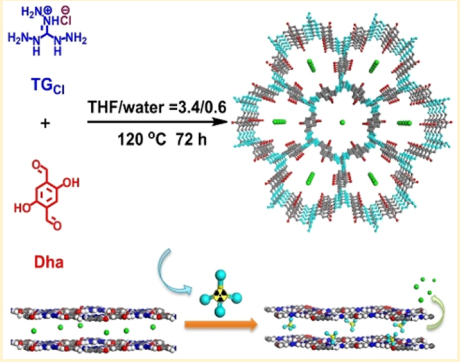

INTRODUCTION

Nuclear power, as one of the backbones of the major power supplies, provides about 11% of the electricity all around the world.[1] Although its ultrahigh energy density has great potential to meet the ever-increasing energy demand, radioactive Technetium-99 (^{99}Tc) concomitantly generated from the nuclear fuel processing as the fission product of ^{235}U or ^{239}Pu at relatively high yields about 6.1%.[2,3] It is estimated that the inventory of ^{99}Tc was nearly quadrupled between 1994 and 2010.[4] Owing to the remarkable radiation dose and extremely long half-life (2.13×10^5 years), ^{99}Tc has become the greater environmental concern compared to other radioactive elements, such as ^{90}Sr and ^{137}Cs.[5] ^{99}Tc mainly exists in the most stable +7 oxidation state as the pertechnetate anion (TcO_4^-) under different conditions, but it shows relatively low reactivity and is not a strong oxidant.[6] The high solubility in water (11.3 mol L^{-1} for the sodium salt) and noncomplexing property make TcO_4^- easily migrate in the subsurface and hard to be immobilized during waste disposal.[7] Meanwhile, the system construction of vitrification facilities is also a significant challenge due to the generation of volatile Tc (VII) during waste typical vitrification process.[8] Therefore, it is critical to exploit superior materials to capture radioactive TcO_4^- before the vitrification of nuclear waste.

Ion exchange has attracted the most interests for TcO_4^- sequestration to date because of its easy implementation and high recovery of targeted anions.[9,10] Over the last decades, many ion exchangers have been used to remove TcO_4^- from Hanford tank wastes.[9,12−14] The commercialized polymeric exchange resins, such as Reillext-HPQ and SuperLig 639, have been widely used as the adsorbents for ^{99}Tc removal in large scale waste treatment.[11,15] Other examples of traditional ion exchangers for TcO_4^- removal involve inorganic cationic materials such as layered double hydroxides (LDH, e.g. Mg−Al LDH, Ni−Al-LDH, $Y_2(OH)_5Cl{\cdot}1.5H_2O$),[12,16] chalcogels ($PtGe_2S_5$),[13] and thorium-based material (NDTB-1).[4,14] Unfortunately, most of these materials suffer from slow ion exchange kinetics, poor selectivity, and low capacity due to their low surface area, uneven pore distribution, hydrophilic surface, and low structural stability.

Cationic metal organic frameworks (MOFs), a new class of crystalline porous materials, have been intensively studied in nuclear waste treatment.[17−22] They are constructed by positively charged networks and noncoordinated anions within

Received: November 6, 2018
Revised: March 28, 2019
Accepted: April 1, 2019
Published: April 1, 2019

DOI: 10.1021/acs.est.8b06244
Environ. Sci. Technol. 2019, 53, 5212−5220

pores or interlayers. Cationic MOFs, such as SCU-100,[23] SCU-101,[24] SCU-102,[25] and UiO-66-$NH_3^+Cl^-$,[26] have shown excellent performance for the removal of TcO_4^- and ReO_4^- (a nonradioactive surrogate of radioactive TcO_4^-). Ag-based MOFs show the most superior uptake capacity to TcO_4^- among these cationic crystalline materials, but the high cost associated with the noble metal and relatively low stability of coordinate bond are unfavorable for practical application in complex aqueous systems.[23,24] A porous aromatic framework (PAF-1) offers remarkable specific surface area to trap ReO_4^-, but the postmodification strategy used to incorporate binding sites of ReO_4^- into the network renders uncontrollable distribution and less loading of functionalities, resulting in low uptake capacity and slow kinetics.[27] Therefore, new types of adsorbents with the traits of fast kinetics, high uptake capacity, low-cost, and good stability are urgently needed for TcO_4^- removal. Very recently, a cationic polymer SCU-CPN-1 with abundant cationic organic fragments linked by covalent bonds was reported as the most efficient TcO_4^- adsorbent with a high uptake capacity of 999 mg L^{-1}.[28]

ReO_4^- is often used as a nonradioactive surrogate to mimic the anion exchange behaviors of radioactive TcO_4^- owing to their similar electronic distribution, spatial configuration, and thermodynamic parameters.[29,30] The most effective approach to achieve strong binding with TcO_4^- or ReO_4^- is to exploit Coulombic interactions because of its noncomplexing nature and the most stable form of TcO_4^- or ReO_4^- under various conditions.[31] Based on the oxo-anion nature of TcO_4^- or ReO_4^-, hydrogen bond interaction has also been employed to adsorb such radioactive pollutants.[32,33] Therefore, the incorporation of positive charged fragments with abundant hydrogen bonding donors in the skeleton would generate effective adsorbents for radioactive anions. Meanwhile, considering the intrinsic properties of large size and low charge density of TcO_4^- or ReO_4^-, it is better to integrate soft-acid fragment as binding sites in adsorbents, such as polycations or structures containing guanidine groups.[34] Moreover, the hydrophobic surface would be beneficial to the diffusion of TcO_4^- or ReO_4^- anions within the pores as the TcO_4^- and ReO_4^- are more hydrophobic than other typical inorganic anions.[29,35] Based on the above criterions, cationic covalent organic frameworks (iCOFs),[36−40] a different type of porous crystalline polymers equipped with ionic building blocks, would be good candidates as adsorbents for the capture of nuclear waste oxo-anions.

iCOFs, which consist of positive charged organic units and weakly bonded anions within pores or interlayers, are a less studied subclass of COFs with unusual electrostatic functions.[36,37] The flexibly tunable structures of iCOFs enable precise integration of abundant predesignable ionic sites into skeletons. The linking of rigid organic units with robust covalent bonds gives higher chemical stability to iCOFs than cationic MOFs and polymer resins.[41] Well-defined hydrophobic porous channels of iCOFs are favorable for more hydrophobic anions diffusion.[29−35] Incorporation of positively charged building blocks as knots would induce self-exfoliation to few layered cationic covalent organic nanosheets (iCONs) via strong interlayer repulsion,[43] which can expose more ionic sites to target objects and give faster ion diffusion dynamics.[40] Currently, the superior performance for organic dyes or $KMnO_4$ removal have been achieved with diverse iCOFs through anion exchange process.[36−40] Recently, a two-dimensional iCOF SCU-COF-1 was reported for TcO_4^- removal with fast adsorption kinetics, ultrahigh uptake capacity and good anion-exchange selectivity.[42] However, the development of iCONs for the capture of TcO_4^- or ReO_4^- has not been reported so far.

Herein, we report the design and synthesis of an iCON $DhaTG_{Cl}$ from 2,5-dihydroxyterephthalaldehyde (Dha) and triaminoguanidinium chloride (TG_{Cl}) for rapid and selective trapping of ReO_4^- anions. $DhaTG_{Cl}$ shows ultrafast exchange kinetics with a maximum uptake capacity of 437 mg g^{-1} for ReO_4^- at room temperature without shaking, much faster than the industrial resins Purolite A520E and IRA-401, leading materials used for the alkaline tank wastes at the Hanford Sites.[10] The performance of $DhaTG_{Cl}$ for ReO_4^- adsorption is negligibly affected over a wide pH range from 3 to 12. About 73% of ReO_4^- could be removed by $DhaTG_{Cl}$ under the complex simulated Hanford Law stream sample. The anion exchange process and hydrogen bonding account for the strong affinity of cationic $DhaTG_{Cl}$ to ReO_4^-. The results reveal the potential application of the iCON to the treatment of pertechnetate from contaminated groundwater.

MATERIALS AND METHODS

Synthesis of Cationic $DhaTG_{Cl}$. $DhaTG_{Cl}$ was synthesized via Schiff reaction between 2,5-dihydroxyterephthalaldehyde (Dha, 0.3 mmol) and triaminoguanidinium chloride (TG_{Cl}, 0.2 mmol) in 4 mL of tetrahydrofuran (THF)/water (3.4:0.6, v/v). The mixture was placed into a 35 mL Schlenk tube (length 125 mm, o.d. Twenty-six mm) and sonicated for 15 min. After the mixture was degassed under liquid N_2 by freeze−pump−thaw cycles for three times, the tube was sealed with screw cap and heated at 120 °C for 3 days. $DhaTG_{Cl}$ was obtained as dark yellow precipitates. The product was collected by centrifugation and washed with THF, *N*,*N*-dimethylformamide (DMF), and anhydrous alcohol and dried at 80 °C under vacuum overnight in ca. 92% isolated yield. FT−IR: 3421, 3248, 1624, 1440, 1326, 1196, 1167, 1096, 957, 882 cm^{-1}. PXRD: 5.2°, 27.3°.

Anion Exchange Studies. All the adsorption processes were carried out with the solid/liquid ratio of 1 mg mL^{-1} at 25 °C. In a typical process, 4 mg of $DhaTG_{Cl}$ was added into a 4 mL aqueous solution with certain content of ReO_4^- in a vial. The equilibrated mixtures were separated by a 0.22 μm PES filter after a certain contact time. The concentrations of ReO_4^- after adsorption were determined by inductively coupled plasma atomic emission spectrometry (ICP-AES). After ion exchange, the solids were washed with ultrapure water and vacuum-dried, then characterized by PXRD, FT−IR, XPS, and SEM-EDS. The distribution coefficient K_d was obtained according to the equation of $K_d = [(C_0-C_e)\ V/C_e]/m$, C_0, and C_e are the initial and equilibrium concentration of ReO_4^-, V is the total volume of solution, m is the mass of the sorbent.

Desorption Experiments. The $DhaTG_{Cl}$-ReO_4^- was obtained by immersing 8 mg $DhaTG_{Cl}$ in 8 mL 100 mg mL^{-1} of ReO_4^- for 2 h. A certain amount of NaCl desorption solution was added into a glass vial containing 4 mg preadsorbed material. After desorbing for a predetermined time, the solid adsorbent was centrifuged at 8000 rpm for 5 min. The concentration of ReO_4^- in the filter liquor was determined by ICP-AES. The same procedure was repeated to optimize the concentration, volume, time and number of desorption cycles involved in the desorption of ReO_4^- from $DhaTG_{Cl}$-ReO_4^-. Finally, the desorbed compound was washed for several times with ultrapure water and dried for reuse.

DOI: 10.1021/acs.est.8b06244
Environ. Sci. Technol. 2019, 53, 5212−5220

Reusability. To study the reusability of $DhaTG_{Cl}$, 100 mg L^{-1} of ReO_4^- solution was used at the solid/liquid ratio of 1 mg mL^{-1} for presorption. The adsorbed ReO_4^- was eluted with 1 mL of 0.5 M NaCl solution. The regenerated material was then added to the fresh ReO_4^- solutions for 2 h and the residual concentrations of targets were measured by ICP-AES.

Anion Competition Experiments. To investigate the exchange selectivity of prepared material, 0.5 mmol L^{-1} competing anions (NO_3^-, SO_4^{2-}, CO_3^{2-}, and PO_4^{3-}) were separately mixed with 0.5 mmol L^{-1} ReO_4^- solutions, then 4 mg $DhaTG_{Cl}$ were added in four parallel cuvettes without shaking for 2 h at 25 °C. After filtration, ICP-AES was utilized to monitor the concentrations of ReO_4^- in the final solutions and IC was used to monitor the concentrations of competing anions. Above process was then repeated with resins under the same conditions as comparison. Effect of NO_3^- and SO_4^{2-} on anion exchange process were further investigated by adding different concentrations of NO_3^- or SO_4^{2-} into ReO_4^- solutions.

RESULTS AND DISCUSSION

Synthesis and Characterization of $DhaTG_{Cl}$. In response to the urgent need for highly efficient adsorbents to trap anionic radioactive pollutants, we directly implant cationic soft-acid guanidine moieties into the framework to produce novel functions including strong affinity to ReO_4^-, positive charge integrity over a wide pH range and self-exfoliation of the final material. Figure 1a illustrates the scheme for the synthesis of $DhaTG_{Cl}$ (see the Supporting Information (SI) for more details). The guanidine unit TG_{Cl} was successfully synthesized from guanidinium chloride in 1,4-dioxane under refluxing (SI Figures S1 and S3), then condensed with Dha in the appropriate solvent to form $DhaTG_{Cl}$. The chloride ions loosely interact with guanidine units as charge-balancing anions (Figure 1b). The weak interaction of chloride ions with the skeleton is conductive to be exchanged out by ReO_4^-. Although all the organic units are planner, cationic layers with loosely bonded chloride ions between them construct weak stacking, motivating intrinsic self-exfoliation of original bulk COF to iCON.[43] The excellent self-exfoliating property of 2D matrix increases the number of cationic sites available for anion sorption. For another organic unit, the hydroxyl group in Dha provides sites for hydrogen bonding to improve the crystallinity of iCON via hydrogen bonds[44] and the affinity of $DhaTG_{Cl}$ to oxo-anions (Figure 1c).[32,33]

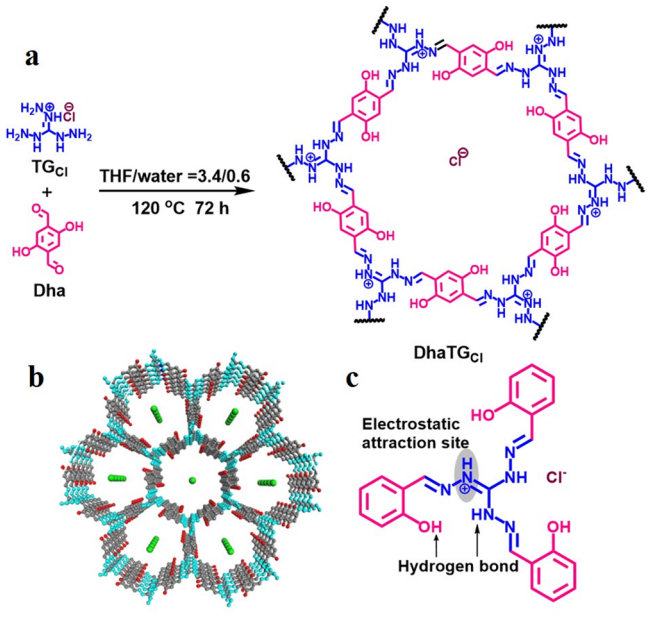

Figure 1. (a) Synthetic scheme of $DhaTG_{Cl}$ through the condensation of TG_{Cl} and Dha; (b) Graphic view of $DhaTG_{Cl}$ in the eclipsed AA stacking model (blue, N; gray, C; red, O; white, H); (c) Illustration of the adsorption interactions between $DhaTG_{Cl}$ and oxo-anions (ReO_4^-) via electrostatic attraction and hydrogen bonding.

The reaction conditions including solvent composition, reaction time and temperature play important roles in the preparation of $DhaTG_{Cl}$. Suitable combination of different solvents in a proper ratio is the key to the generation of crystalline frameworks. Due to the excellent water solubility of TG_{Cl}, we chose water as a main solvent and its combination with THF, 1,4-dioxane or ethanol as binary solvent systems. The combination of water and THF gave the best crystalline polymer (Figure S4). In addition, a binary solvent of water and THF (3.4/0.6 v/v) led to relatively high crystallinity of $DhaTG_{Cl}$ (SI Figure S5). Higher temperature is also of assistance to the formation of ordered and crystalline structures (SI Figure S6). An increase of reaction time to 60 h obviously improved the peak intensity at 5.2°, demonstrating that sufficient reaction time is necessary to generate crystalline framework (SI Figure S7). Thus, the dark-yellow $DhaTG_{Cl}$ powder with the yield of ca. 92% was synthesized from Dha and TG_{Cl} in the mixture of THF/water (3.4/0.6, v/v) at 120 °C for 72 h.

The structure of the as-prepared $DhaTG_{Cl}$ was analyzed on the basis of PXRD pattern, structural simulation and Pawley refinement. The PXRD pattern of the as-prepared $DhaTG_{Cl}$ shows a minor peak at 5.2° (SI Figure S8), corresponding to the reflection of the (100) plane. The second major broad peak at ca. 27.0° implies poor $\pi-\pi$ stacking between the layers in the vertical direction.[40] The above results reveal the successful synthesis of the crystalline network. Similar with the reported structure of $TpTG_{Cl}$,[43] the charge repulsion of cationic guanidine units and loosely sandwiched chloride ions can disturb the $\pi-\pi$ stacking between the layers, posing low crystallinity of the prepared $DhaTG_{Cl}$ nanosheets. Structural simulation of $DhaTG_{Cl}$ was carried out by the Material Studio (ver. 7.0). Based on the few-layered stacking structure of $DhaTG_{Cl}$ obtained by experimental results, we constructed a possible two-dimensional (2D) eclipsed AA stacking mode (Figure 2a and b) with the parameters of $a = b = 20.9189$ Å, $c = 3.5184$ Å, $\alpha = \beta = 90°$, $\gamma = 120°$ (SI Figure S9 and Table S1). The Pawley refinement of AA stacking mode outputted a PXRD profile (SI Figure S10, red curve) which is in good agreement with the experimental PXRD pattern due to their minute difference and relatively low values of Rwp (7.32%) and Rp (5.51%). In contrast, an AB staggered stacking mode (SI Figure S11) gave a PXRD pattern with a great difference from that of experimental profile (Figure 2c). The eclipsed AA-stacking mode could avoid the overlap of chelating sites by adjacent layers such that anions can easily diffuse to binding sites within ordered pore channels.[38]

The FT−IR spectrum of $DhaTG_{Cl}$ (Figure 2d, black curve) exhibits a new stretching vibration band at 1624 cm^{-1}, demonstrating the formation of imine bonds due to the condense between the aldehyde groups of Dha and amino groups of TG_{Cl}.[43] Meanwhile, the absence of the characteristic

DOI: 10.1021/acs.est.8b06244
Environ. Sci. Technol. 2019, 53, 5212−5220

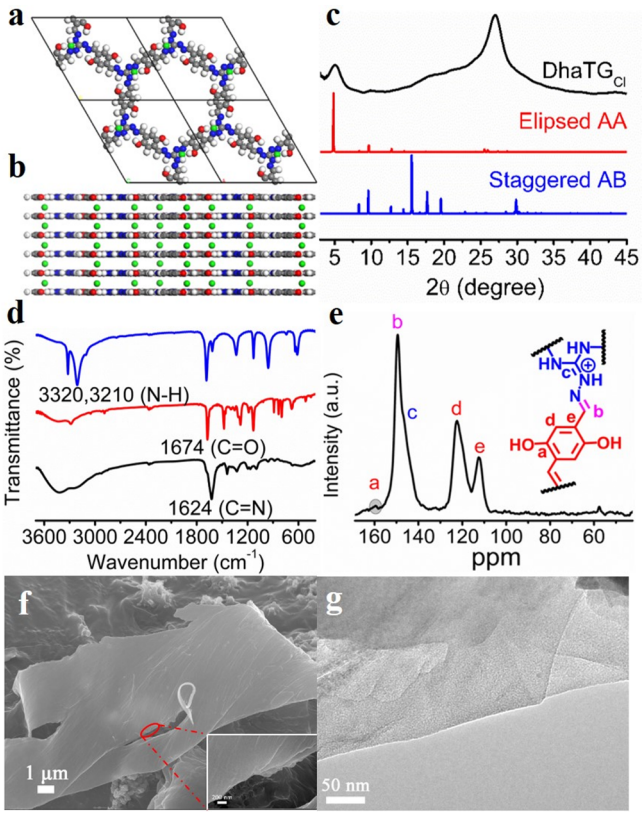

Figure 2. (a) Unit cells of the AA stacking model, and (b) side view of the AA stacking model of DhaTG$_{Cl}$ (C: gray; N: blue; O: red; Cl: green; H: white); (c) Comparison of PXRD profiles of DhaTG$_{Cl}$ between the experimental, the AA eclipsed (simulated) and the AB staggered (simulated) stacking modes; (d) FT−IR spectra of TG$_{Cl}$ (blue curve), Dha (red curve) and DhaTG$_{Cl}$ (black curve); (e) ^{13}C CP MAS solid-state NMR of cationic DhaTG$_{Cl}$; (f) SEM image (inset: edge of nanosheets) and (g) TEM image of DhaTG$_{Cl}$ nanosheets.

peaks at 3320 and 3210 cm^{-1} of N−H (TG$_{Cl}$) (Figure 2d, blue curve) and 1674 cm^{-1} of C = O (Dha) (Figure 2d, red curve) from the initial organic monomers also indicate the generation of imine bonds via the Schiff reaction of TG$_{Cl}$ and Dha. The ^{13}C CP-MAS solid-state nuclear magnetic resonance (NMR) spectra further confirm the chemical structure of DhaTG$_{Cl}$ (Figure 2e). The chemical shifts at 150 and 147 ppm belong to the carbon atoms of the C═N bond formed via Schiff reaction andthe C═N bond of the TG$_{Cl}$ fragment, respectively. The chemical shifts at 114, 122, and 160 ppm are ascribed to the carbons of phenyl groups.[40,43] To further confirm the chemical shifts of ^{13}C CP-MAS NMR spectra for DhaTG$_{Cl}$, the model compound SaTG$_{Cl}$ was synthesized and characterized with ^{13}C NMR and DEPT 135° (SI Figures S12−S14). The peaks at 157, 148, and 119 ppm in ^{13}C NMR spectrum (SI Figure S13) of SaTG$_{Cl}$ disappeared in DEPT 135° spectrum (SI Figure S14), showing that the peaks at 160 and 147 ppm in ^{13}C CP-MAS NMR spectra of DhaTG$_{Cl}$ originated from C(Ar)−OH and C═N of TG$_{Cl}$, respectively. The peak at 149 ppm in ^{13}C NMR spectrum of SaTG$_{Cl}$ remained in DEPT 135° spectrum, demonstrating that the peak at 150 ppm in ^{13}C CP-MAS NMR spectra of DhaTG$_{Cl}$ resulted from CH═N of iCON formed via Schiff reaction.

The porosity and surface area of DhaTG$_{Cl}$ were investigated by nitrogen adsorption−desorption measurements at 77 K. The adsorption isotherms are corresponding to type-II reversible adsorption model (SI Figure S15).[40] The Brunauer−Emmett−Teller (BET) surface area (SI Figure S16) and pore volume of DhaTG$_{Cl}$ are 96 m^2 g^{-1} and 0.44 cc g^{-1}, respectively. The relatively low BET surface area of DhaTG$_{Cl}$ likely resulted from the low crystallinity of prepared DhaTG$_{Cl}$ and the existence of counterion inside the pore channels, which was also observed on CON-Cl.[43] The pore size calculated via the nonlocal density functional theory (NLDFT) method of DhaTG$_{Cl}$ is 1.5 nm (SI Figure S17), which is much larger than the hydrodynamic size of TcO_4^- (2.5 Å) or ReO_4^- (2.6 Å),[11] allowing effective anions transfer within pores. The self-exfoliated DhaTG$_{Cl}$ nanosheets were characterized by field emission scanning electron microscopy (SEM), transmission electron microscopy (TEM), and atomic force microscope (AFM) measurements. SEM (Figure 2f and SI Figure S18) and TEM (Figure 2g and SI Figure S19) images reveal the morphology of DhaTG$_{Cl}$ thin sheets, suggesting the presence of charge repulsion between cationic layers successfully induced the exfoliation. AFM measurement (SI Figure S20) in tapping mode further confirms the obtained DhaTG$_{Cl}$ nanosheets. The height profile of cationic DhaTG$_{Cl}$ nanosheets was around 5 nm in the range of high aspect ratio, implying the iCON were self-exfoliated into 5−7 layers.[45,46]

The chemical stability of DhaTG$_{Cl}$ in aqueous system was evaluated by dispersing DhaTG$_{Cl}$ in water in a pH range of 3−12 at 25 °C for 2 days. No obvious change in the PXRD pattern was observed (SI Figure S21), indicating that the crystalline framework is resistant in the pH range of 3−12. The high structural stability of DhaTG$_{Cl}$ over a wide pH range motivated us to evaluate the performance of DhaTG$_{Cl}$ for radioactive oxo-anions removal.

Adsorption Performance of DhaTG$_{Cl}$ Nanosheets for ReO_4^-. To access the anion exchange performance, the DhaTG$_{Cl}$ nanosheets were mixed with the ReO_4^- solutions at initial concentrations ranging from 25 to 500 mg L^{-1} at 25 °C under neutral condition. The concentrations of ReO_4^- in solutions were measured by ICP-AES as a function of time. As shown in Figure 3a, the ReO_4^- in the solution (initial concentration, 25 mg L^{-1}) was quickly reduced by 98.0% and 99.1% in 5 and 30 min, respectively, showing the ultrafast adsorption kinetics of DhaTG$_{Cl}$ for ReO_4^-. UV−vis adsorption spectra were used to monitor anion exchange process due to the characteristic adsorption of 25 mg L^{-1} ReO_4^- at 230 nm.[7] The results also confirm the ultrafast kinetics of anion exchange process with the rapidly decreased adsorption intensity at 230 nm (Figure 3b). DhaTG$_{Cl}$ gave faster adsorption of ReO_4^- than cationic MOFs SCU-100 and SCU-101 with Ag^+ sites (SI Table S2). This ultrafast adsorption kinetics is vital since several hours are required to reach exchange equilibrium for previous anion exchangers including NDTB-1,[6,14] UiO-66-$NH_3^+Cl^-$[26] and PAF-1[27] under the same conditions.

Two commercial anion exchange resins including A520E and IRA-401 with high uptake capacity for TcO_4^- were selected for further comparison.[9,11] Figure 3c shows that DhaTG$_{Cl}$ rendered much faster adsorption kinetics than A520E and IRA-401. 94.0% of ReO_4^- in the solution (initial concentration, 100 mg L^{-1}) was removed by DhaTG$_{Cl}$ in 5 min whereas only 85.42% and 73.65% of ReO_4^- were captured by A520E and IRA-401, respectively, after 24 h adsorption. In addition, the adsorption equilibrium time of A520E and IRA-401 for ReO_4^- was about 60 and 72 h, respectively (SI Table

DOI: 10.1021/acs.est.8b06244
Environ. Sci. Technol. 2019, 53, 5212−5220

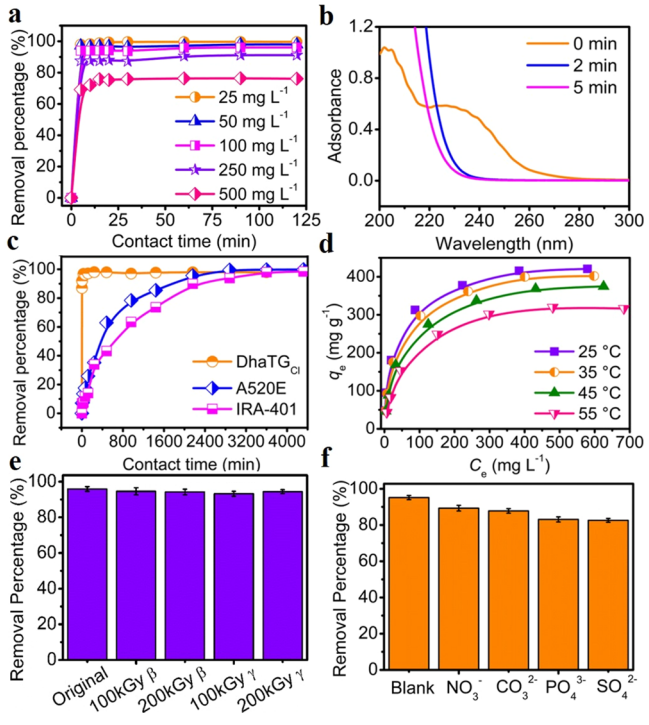

Figure 3. (a) Adsorption kinetics of $DhaTG_{Cl}$ for ReO_4^- at initial concentrations of 25 mg L^{-1} to 500 mg L^{-1}; (b) Time-dependent UV−vis spectra of ReO_4^- solution (initial concentration: 25 mg L^{-1}) on $DhaTG_{Cl}$ at 25 °C; (c) Comparison of adsorption kinetics of $DhaTG_{Cl}$, Purolite A520E and IRA-401 for ReO_4^- (100 mg L^{-1}) at 25 °C; (d) Adsorption isotherms of $DhaTG_{Cl}$ for ReO_4^- from 25 to 55 °C; (e) Removal percentage of ReO_4^- (100 mg L^{-1}) before and after irradiated by β-rays and γ-rays; (f) Effect of typical competing oxo-anions (0.5 mmol L^{-1}) on the removal percentage of ReO_4^- (initial concentration of ReO_4^-: 0.5 mmol L^{-1}) at 25 °C; (solid/liquid = 1:1, mg/mL for all)

S3). This phenomenon should be in part attributed to the structural advantage of few-layered stacking $DhaTG_{Cl}$ nanosheets with well-defined and inerratic hydrophobic porosity, inducing more effective ReO_4^- anion transfer than amorphous anion exchange resins with uneven pore distribution. Aside from porous structure, the relatively compact pore size of $DhaTG_{Cl}$ is favorable for effective anion diffusion compared to typical resins with larger pore size.[23] The ultrafast exchange kinetics is a significant property to dramatically reduce time to expose the adsorbents in harsh conditions, increasing the likelihood of structural retention during waste treatment.

Batch experiments were performed to further understand the ion exchange process of $DhaTG_{Cl}$ for ReO_4^-. The anion exchange kinetics of ReO_4^- on $DhaTG_{Cl}$ followed a pseudo-second-order model, indicating the chemical adsorption dominated the adsorption process of $DhaTG_{Cl}$ for ReO_4^- (SI Figure S22 and Table S3).[47] The adsorption isotherms of $DhaTG_{Cl}$ were well fitted by Langmuir model (Figure 3d and SI Figure S23) with good determination coefficient (R^2 > 0.998) (SI Table S4), suggesting that the uniform and monolayer adsorption model was more appropriate for the adsorption of ReO_4^- on $DhaTG_{Cl}$.[47] The calculated thermodynamic parameters (SI Figure S24 and Table S5) reveal that the exchange process of ReO_4^- on $DhaTG_{Cl}$ is spontaneous. Increase of temperature reduced the adsorption capacity, implying the adsorption process of ReO_4^- on $DhaTG_{Cl}$ is exothermic.

The saturation adsorption capacity is 437 mg g^{-1}at 25 °C (SI Table S4), higher than those of inorganic cationic material Mg−Al LDH (130.2 mg g^{-1}), MOFs SCU-101 (271 mg g^{-1}), UiO-66-$NH_3^+Cl^-$ (159 mg g^{-1}), SCU-102 (291 mg g^{-1}), and amorphous porous aromatic frameworks PAF-1 (420 mg g^{-1}),[24−27] but lower than those of MOFs SCU-100 (541 mg g^{-1}),[23] SLUG-21 (607 mg g^{-1}),[48] SCU-COF-1 (702.4 mg g^{-1}),[42] SBN (786 mg g^{-1})[22] and SCU-CPN-1 (999 mg g^{-1})[28] (SI Table S6). The distribution coefficient value (K_d) is often used to access the interaction between the sorbents and targets.[49] The K_d of $DhaTG_{Cl}$ toward ReO_4^- at 25 °C is 5.0 × 10^5 mL g^{-1} (SI Table S7), which ranks one of the highest values and competes with the K_d values of reported novel materials, including SCU-101 (7.5 × 10^5 mL g^{-1}),[24] SCU-102 (5.6 × 10^5 mL g^{-1}),[25] SCU-COF-1 (3.89× 10^5 mL g^{-1}),[42] SCU-CPN-1 (6.5 × 10^5 mL g^{-1}),[28] SCU-100 (1.9 × 10^5 mL g^{-1}),[23] and PAF-1 (2.55 × 10^4 mL g^{-1}).[27] Compared to the commercial resins tested in this work, the K_d value of $DhaTG_{Cl}$ is close to the value of Purolite A520E (7.6 × 10^5 mL g^{-1}) and ten times higher than IRA-401 (6.3 × 10^4 mL g^{-1}), indicating the strong affinity is achieved between $DhaTG_{Cl}$ and ReO_4^- anions via implanting guanidine groups and hydrogen bond sites to scaffolds. $DhaTG_{Cl}$ gave the equilibrium concentration of ReO_4^- in solution comparable to the commercialized resin Purolite A520E and IRA-401, and lower than SCU-100 (SI Table S8).

The capture of ReO_4^- in a wide pH range is highly desirable for practical waste disposal. The effect of pH on the ion exchange of ReO_4^- was studied in the pH range of 3−12 (SI Figure S25). The exchange efficiencies of $DhaTG_{Cl}$ for ReO_4^- were kept about 95% over a pH range of 3−12 due mainly to the strong basicity of the guanidine units (pK_a = 13.6).[50] The pK_a value of $HReO_4$ is −0.28,[11] leading to negatively charged ReO_4^- in the pH range of 3−12. The above results show that the electrostatic interaction can be preponderant between ReO_4^- and $DhaTG_{Cl}$. Furthermore, ^{60}Co γ and β irradiation (10 MeV) did not impair the crystal structure (SI Figure S26) and the adsorption capacity (Figure 3e) of $DhaTG_{Cl}$, demonstrating the good radiation resistance of $DhaTG_{Cl}$.

The desorption of ReO_4^- from $DhaTG_{Cl}$ was studied using aqueous solution of NaCl as the solvent (SI Figures S27−S29). Optimization of the concentration (0.5−3.0 mol L^{-1}) and the volume (1−6 mL) of NaCl solution, the time (2−60 min) and the cycle number (1−4) for desorption led to the desorption of about 98% of the adsorbed ReO_4^- by 10 min rinsing with 1 mL of 0.5 mol L^{-1} NaCl for four times. No significant decrease in the adsorption capacity of $DhaTG_{Cl}$ for ReO_4^- (100 mg L^{-1}) was found even after five adsorption−desorption cycles (SI Figure S29), underlining its good reusability for ReO_4^- removal.

Adsorption Selectivity. The ion exchange selectivity is another important parameter for efficient capture of targeted anions. This factor was investigated by placing $DhaTG_{Cl}$ into a mixture containing 0.5 mmol L^{-1} four kind of typical competing anions (NO_3^-, CO_3^-, PO_4^{3-} and SO_4^{2-}) and 0.5 mmol L^{-1} ReO_4^-. The removal percentage is 97.1% when the solid to liquid ratio of $DhaTG_{Cl}$ to ReO_4^- was 5 mg mL^{-1}. The uptake of ReO_4^- was further studied in the presence of NO_3^-, CO_3^-, PO_4^{3-} and SO_4^{2-}, respectively. More than 82% of ReO_4^- was removed when the ratio of solid to liquid was 1 mg mL^{-1} for all four anions (Figure 3f). $DhaTG_{Cl}$ gave much better anion selectivity than typical commercialized resins A520E and IRA-401 (SI Table S8). In the most cases, anions

DOI: 10.1021/acs.est.8b06244
Environ. Sci. Technol. 2019, 53, 5212−5220

with higher charge density induce the reduction of the standard hydration Gibbs energies (ΔG_h^0), which is in favor of anion extraction from the water.[51] In this case, ReO_4^- anions were selectively adsorbed on $DhaTG_{Cl}$ in the presence of NO_3^-, PO_4^{3-}, and SO_4^{2-} because the stronger interactions between the low positive charge density of the guanidine-based iCON and the lower negative charge density of ReO_4^- than competing anions.[7,52] The interaction of competing oxo-anions with $DhaTG_{Cl}$ follows a decreasing order of SO_4^{2-} > PO_4^{3-} > CO_3^{2-} > NO_3^-. This phenomenon follows the principle of anti-Hofmeister bias due probably to hydrophobic nature of the $DhaTG_{Cl}$ skeleton (SI Figure S30).[23,51] The removal efficiency of ReO_4^- was still up to 80% at the NO_3^- to ReO_4^- molar ratio of 20:1 (Figure 3a). Over 10-fold the concentration of ReO_4^-, SO_4^{2-} made the removal percentage of ReO_4^- decrease more than NO_3^- and CO_3^- (SI Figure S31). Lager anions are softer bases, and more favorably bind soft acid guanidinium sites to compete with ReO_4^- than smaller anions, so SO_4^{2-} (r = 0.230 nm) with smaller difference in size from ReO_4^- had more negative effect on the removal of ReO_4^- than NO_3^- (r = 0.200 nm) and CO_3^- (r = 0.189 nm).[53]

The effect of Ca^{2+} and Mg^{2+} on ReO_4^- removal were studied at various Ca^{2+} and Mg^{2+} to ReO_4^- molar ratio (SI Figure S32). The removal percentage of ReO_4^- had no significant change in the presence of 10-fold Ca^{2+} or Mg^{2+} and was still over 80% even in the presence of 100-fold Ca^{2+} or Mg^{2+}. However, the presence of too high concentration (1000 folds) of Ca^{2+} or Mg^{2+} reduced the removal percentage of ReO_4^- to about 60% due to the affinity of these hard metal ions to oxygen-containing groups in $DhaTG_{Cl}$.[52]

ReO_4^- Removal from a Simulated Sample. A simulated Hanford LAW Melter recycle Stream was used to further reveal the potential of $DhaTG_{Cl}$ for the application in nuclear waste treatment.[14] ReO_4^- was used instead of radioactive TcO_4^- anion as a nonradioactive surrogate to avoid handing radioactive TcO_4^- in a conventional lab. Although the interfering concentrations of NO_3^-, NO_2^- and Cl^- are much higher than targeted ReO_4^- anion (SI Table S10), 73.7% of ReO_4^- in the simulated stream was still removed by $DhaTG_{Cl}$ when the solid to liquid ratio was 5 mg mL^{-1}, revealing the great potential of $DhaTG_{Cl}$ in nuclear waste treatment.

Adsorption Mechanism. The superior adsorption performance motivates us to further explored the adsorption mechanism. Element mapping profiles reveal that Re element uniformly and extensively dispersed within ReO_4^--loaded $DhaTG_{Cl}$ (SI Figure S33). Meanwhile, a new peak at 909 cm^{-1} in the FT−IR spectra appeared after the adsorption of ReO_4^- (Figure 4a), corresponding to the stretching vibration of Re−O bond involved in $DhaTG_{Cl}$-ReO_4^-.[23] The red shift (ca. 16 cm^{-1}) of the characteristic peaks for N−H and O−H stretching vibration at 3340 cm^{-1}, and the decrease of the N−H stretching intensity at 1656 cm^{-1}, as well as a new broad peak at 3241 cm^{-1} for the formation of NH-O bond demonstrate that guanidine and hydroxyl groups were involved in strong interactions between $DhaTG_{Cl}$ and ReO_4^-.[54] The overlaid spectra of XPS analysis are consistent with the occurrence of anion exchange process as the original peak of Cl 2p almost vanished and a new peak of Re 4f appeared in $DhaTG_{Cl}$-ReO_4^- (SI Figure S34). To further verify the roles of guanidine groups and hydroxyl groups in the adsorption process of ReO_4^-, the N 1s and O 1s core-level spectra of $DhaTG_{Cl}$ and $DhaTG_{Cl}$-ReO_4^- were analyzed. The N 1s core

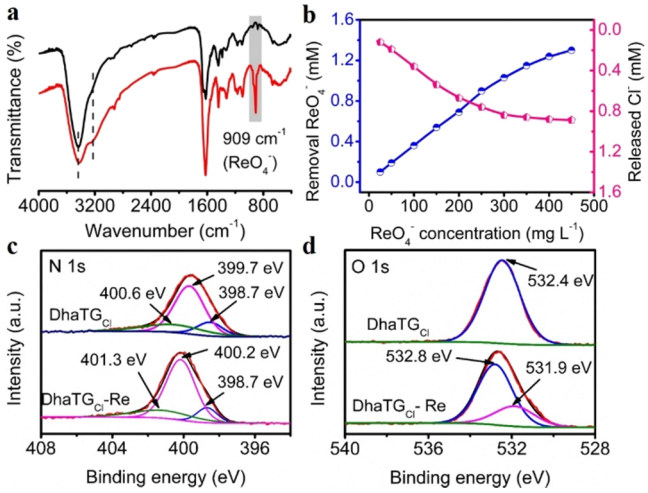

Figure 4. (a) Comparison of FT−-IR spectra of $DhaTG_{Cl}$ before (black curve) and after (red curve) adsorption with ReO_4^-; (b) Dependence of the concentration of removed ReO_4^- and released Cl^- from $DhaTG_{Cl}$ on the initial concentration of ReO_4^-. (solid/liquid = 1:1, mg/mL) (blue curve: removed ReO_4^-; pink curve: released Cl^-); XPS spectra of (c) N 1s and (d) O 1s of fresh $DhaTG_{Cl}$ and $DhaTG_{Cl}$-ReO_4^-.

level of = N− (398.7), −NH− (399.7 eV) and protonated = $^+$NH− (400.6 eV) is shifted to higher binding energy after ReO_4^- loading (400.2 eV for −NH− and 401.3 eV for = $^+$NH−) (Figure 4c).[55,56] The N 1s core level shifted more in = $^+$NH− (0.7 eV) compared to 0.5 eV in −NH−, implying that cationic moieties of = $^+$NH− have stronger interactions with target anions. Besides, the hydroxyl groups were also involved in adsorption process as the O 1s peak of −OH, positioned at 532.4 eV in the as-prepared state, was positively shifted to 532.8 eV in $DhaTG_{Cl}$-ReO_4^- (Figure 4d). These results confirm the interactions between guanidine or hydroxyl groups and ReO_4^-.

To further confirm the anion exchange process, $DhaTG_{Cl}$ was immersed into ReO_4^- solutions with different concentrations ranging from 0 to 450 mg L^{-1}. The equilibrium concentrations of exchanged-out chloride ions increased at the higher initial concentration of ReO_4^- solution (Figure 4b, pink curve), revealing the anion exchange process occurred between the chloride ions and ReO_4^-. The molar ratio of the adsorbed ReO_4^- to exchanged-out Cl^- was approximately 1:1 when the concentrations were lower than 300 mg L^{-1}. The concentrations of exchanged-out Cl^- started to be lower than that of captured ReO_4^- when the initial concentrations of ReO_4^- were higher than 350 mg L^{-1} (Figure 4b), but the removal efficiency of ReO_4^- kept increasing (Figure 3d, purple curve). This phenomenon suggests that anion exchange should not be the only the mechanism for the adsorption, which was verified by FT−IR and XPS analysis (Figures 4a,c,d). The peak position and intensity of $DhaTG_{Cl}$ after anion exchange are comparable to the fresh ones in PXRD patterns, indicating the lattice retainment of $DhaTG_{Cl}$ during the anion exchange (SI Figure S35).[39] These results show that the size of ReO_4^- (r = 0.260 nm) is not large enough to obviously disturb the $\pi-\pi$ interactions between layers. The ionic radius of ReO_4^- (r = 0.260 nm) is the largest anion among the studied competing anions, including SO_4^{2-} (r = 0.230 nm), NO_3^- (r = 0.200 nm), CO_3^- (r = 0.189 nm). The difference in ion radii radius (DIR) of ReO_4^-/Cl^- is 51.2%.[53] Therefore, the lattice of $DhaTG_{Cl}$

DOI: 10.1021/acs.est.8b06244
Environ. Sci. Technol. 2019, 53, 5212−5220

may not be changed when the DIR is lower than 51.2%. Chen et al.[39] found that the intensity of the broad peak at $2\theta = \sim 28°$ of guanidine-based CON-Cl decreased substantially after exchanging by $TFSI^-$ ions (longest size: $r = 0.395$ nm) while the peak position was still the same, reflecting that the introduction of large sized $TFSI^-$ into iCON can disturb the weak $\pi-\pi$ stacking interactions between layers. So, the distance between layers (parameter c) can be changed if the size of anions is large enough. Such an anion exchange process can be driven by the differences in concentration, interaction and hydration energy.[S1] Much higher concentration of ReO_4^- around the Cl^- in $DhaTG_{Cl}$ is favorable for the exchange process. Larger ReO_4^- ($r = 0.260$ nm), a softer base than smaller Cl^- ($r = 0.172$ nm),[S3,S7] preferentially binds to the soft acid sites (guanidinium) in $DhaTG_{Cl}$.[7] The lower hydration energy of ReO_4^- (-330 kJ mol^{-1}) than Cl^- (-347 kJ mol^{-1}) makes the transportation of ReO_4^- within hydrophobic pore channels more thermodynamically favorable.[S1] Although superhydrophilic guanidine fragments exist in the skeleton of $DhaTG_{Cl}$, hydrophobic surface can be successfully constructed by implanting aromatic substituents in the skeleton (SI Figure S30), which is favorable for ReO_4^- anion diffusion.

To better understand the importance of cationic sites and hydrogen bond interactions in ReO_4^- removal, COF-LZU1 with similar pore structure to $DhaTG_{Cl}$ but without guanidine and hydroxyl groups was synthesized for comparison (SI Figures S2, S36, and S37). After immersing 10 mg of COF-LZU1 in 4 mL of ReO_4^- solution (50 mg L^{-1}) for 24 h, only 5% of ReO_4^- were removed (SI Figure S38), suggesting that the absence of cationic sites and hydrogen bonding sites in the network led to very low ReO_4^- uptake. Although the hydrophobic property of COF-LZU1 was stronger than that for $DhaTG_{Cl}$ (SI Figure S30), the uptake capacity and kinetics were extremely poor. The above results show that the cationic sites coupled with hydrogen binding sites played important roles in ReO_4^- removal. Guanidine-based cations, as large organic cations, have stronger affinity to ReO_4^- with larger molecular size and lower charge density. In addition, the formation of multiple hydrogen bonding interactions, supplied by guanidine groups and Dha, also complement the obvious electrostatic interactions.

In conclusion, we have reported the rational synthesis of a new guanidine-based iCON for efficient removal of radioactive contaminants. Considering the unique advantages of high stability, ordered hydrophobic pore channels and densely accessible cationic sites, our iCON $DhaTG_{Cl}$ has ultrafast anion exchange kinetics over the extensively investigated anion exchangers, such as A520E, IRA-401, and LDHs, even comparable to the novel MOFs with noble metal Ag^+ sites. $DhaTG_{Cl}$ also achieves promising features including high efficiency, good selectivity, excellent pH resistance and reusability. This work will greatly promote further investigation of iCONs with various types of binding sites to exploit their anion trapping properties for the removal of various oxoanionic pollutants and to broaden the potential application of iCONs in the pretreatment of radioactive pertechnetate from contaminated groundwater.

■ ASSOCIATED CONTENT

Supporting Information

The Supporting Information is available free of charge on the ACS Publications website at DOI: 10.1021/acs.est.8b06244.

Additional data including preparation and characterization of organic ligand and COF-LZU1, the sorption isotherm models, adsorption properties, PXRD patterns and adsorption mechanism (PDF)

■ AUTHOR INFORMATION

Corresponding Author

*E-mail: xpyan@jiangnan.edu.cn and xpyan@nankai.edu.cn.

ORCID

Cheng-Xiong Yang: 0000-0002-0817-2232

Xiu-Ping Yan: 0000-0001-9953-7681

Notes

The authors declare no competing financial interest.

■ ACKNOWLEDGMENTS

This work was supported by the National Basic Research Program of China (Grant 2015CB932001), National Natural Science Foundation of China (Grant 21775056 and 21777074), the National First-class Discipline Program of Food Science and Technology (No. JUFSTR20180301), and the Fundamental Research Funds for Central Universities (Grant JUSRP51714B).

■ REFERENCES

(1) Zhang, X.; Silva, I. d.; Godfrey, H. G. W.; Callear, S. K.; Sapchenko, S. A.; Cheng, Y.; Vitórica-Yrezábal, I.; Frogley, M. D.; Cinque, G.; Tang, C. C.; Giacobbe, C.; Dejoie, C.; Rudić, S.; Ramirez-Cuesta, A. J.; Denecke, M. A.; Yang, S.; Schröder, M. Confinement of iodine molecules into triple-helical chains within robust metal-organic frameworks. *J. Am. Chem. Soc.* **2017**, *139* (45), 16289−16296.

(2) Li, B.; Dong, X.; Wang, H.; Ma, D.; Tan, K.; Jensen, S.; Deibert, B. J.; Butler, J.; Cure, J.; Shi, Z.; Thonhauser, T.; Chabal, Y. J.; Han, Y.; Li, J. Capture of organic iodides from nuclear waste by metal-organic framework-based molecular traps. *Nat. Commun.* **2017**, *8*, 485.

(3) Smith, F. N.; Taylor, C. D.; Um, W.; Kruger, A. A. Technetium incorporation into goethite (α-FeOOH): an atomic-scale investigation. *Environ. Sci. Technol.* **2015**, *49* (22), 13699−13707.

(4) Icenhower, J. P.; Qafoku, N. P.; Zachara, J. M.; Martin, W. J. The biogeochemistry of technetium: A review of the behavior of an artificial element in the natural environment. *Am. J. Sci.* **2010**, *310* (8), 721−752.

(5) Lee, M. S.; Um, W.; Wang, G.; Kruger, A. A.; Lukens, W. W.; Rousseau, R. V.; Glezakou, A. Impeding ^{99}Tc (IV) mobility in novel waste forms. *Nat. Commun.* **2016**, *7*, 12067.

(6) Yu, P.; Wang, S.; Alekseev, E. V.; Depmeier, W.; Hobbs, D. T.; Albrecht-Schmitt, T. E.; Phillips, B. L.; Casey, W. H. Technetium-99 mas NMR spectroscopy of a cationic framework material that traps TcO_4^- ions. *Angew. Chem., Int. Ed.* **2010**, *49* (34), 5975−5977.

(7) Katayev, E. A.; Kolesnikov, G. V.; Sessler, J. L. Molecular recognition of pertechnetate and perrhenate. *Chem. Soc. Rev.* **2009**, *38*, 1572−1586.

(8) Darab, J. G.; Smith, P. A. Chemistry of technetium and rhenium species during low-level radioactive waste vitrification. *Chem. Mater.* **1996**, *8* (5), 1004−1021.

(9) Banerjee, D.; Kim, D.; Schweiger, M. J.; Kruger, A. A.; Thallapally, P. K. Removal of TcO_4^- ions from solution: materials and future outlook. *Chem. Soc. Rev.* **2016**, *45*, 2724−2739.

(10) Li, J.; Wang, X.; Zhao, G.; Chen, C.; Chai, Z.; Alsaedi, A.; Hayat, T.; Wang, X. Metal-organic framework-based materials: superior adsorbents for the capture of toxic and radioactive metal ions. *Chem. Soc. Rev.* **2018**, *47*, 2322−2356.

(11) Wilmarth, W. R.; Lumetta, G. J.; Johnson, M. E.; Poirier, M. R.; Thompson, M. C.; Suggs, P. C.; Machara, N. P. Review: waste-

pretreatment technologies for remediation of legacy defense nuclear wastes. *Solvent Extr. Ion Exch.* **2011**, *29* (1), 1−48.
(12) Goh, K. H.; Lim, T. T.; Dong, Z. Application of layered double hydroxides for removal of oxyanions: A review. *Water Res.* **2008**, *42* (6), 1343−1368.
(13) Riley, B. J.; Chun, J.; Um, W.; Lepry, W. C.; Matyas, J.; Olszta, M. J.; Li, X.; Polychronopoulou, K.; Kanatzidis, M. G. Chalcogen-based aerogels as sorbents for radionuclide remediation. *Environ. Sci. Technol.* **2013**, *47* (13), 7540−7547.
(14) Wang, S.; Yu, P.; Purse, B. A.; Orta, M. J.; Diwu, J.; Casey, W. H.; Phillips, B. L.; Alekseev, E. V.; Depmeier, W.; Hobbs, D. T.; Albrecht-Schmitt, T. E. Selectivity, kinetics, and efficiency of reversible anion exchange with TcO_4^- in a supertetrahedral cationic framework. *Adv. Funct. Mater.* **2012**, *22* (11), 2241−2250.
(15) Hassan, N. M.; King, W. D.; McCabe, D. J.; Hamm, L. L.; Johnson, M. E. SuperLig® 639 equilibrium sorption data for technetium from hanford tank waste supernates. *Solvent Extr. Ion Exch.* **2002**, *20* (2), 211−226.
(16) Zhu, L.; Zhang, L.; Li, J.; Zhang, D.; Chen, L.; Sheng, D.; Yang, S.; Xiao, C.; Wang, J.; Chai, Z.; Albrecht-Schmitt, T. E.; Wang, S. Selenium sequestration in a cationic layered rare earth hydroxide: a combined batch experiments and exafs investigation. *Environ. Sci. Technol.* **2017**, *51*, 8606−8615.
(17) Mao, C.; Kudla, R. A.; Zuo, F.; Zhao, X.; Mueller, L. J.; Bu, X.; Feng, P. Anion stripping as a general method to create cationic porous framework with mobile anions. *J. Am. Chem. Soc.* **2014**, *136* (21), 7579−7582.
(18) Desai, V.; Manna, B.; Karmakar, A.; Sahuk, A.; Ghosh, S. K. A water-stable cationic metal-organic framework as a dual adsorbent of oxoanion pollutants. *Angew. Chem., Int. Ed.* **2016**, *55* (27), 7811−7815.
(19) Colinas, R.; Silva, R. C.; Oliver, S. R. J. Reversible, selective trapping of perchlorate from water in record capacity by a cationic metal-organic framework. *Environ. Sci. Technol.* **2016**, *50* (4), 1949−1954.
(20) Li, Y.; Yang, Z.; Wang, Y.; Bai, Z.; Zheng, T.; Dai, X.; Liu, S.; Gui, D.; Liu, W.; Chen, M.; Chen, L.; Diwu, J.; Zhu, L.; Zhou, R.; Chai, Z.; Albrecht-Schmitt, T. E.; Wang, S. A mesoporous cationic thorium-organic framework that rapidly traps anionic persistent organic pollutants. *Nat. Commun.* **2017**, *8*, 1354.
(21) Liu, W.; Wang, Y.; Bai, Z.; Li, Y.; Wang, Y.; Chen, L.; Xu, L.; Diwu, J.; Chai, Z.; Wang, S. Hydrolytically stable luminescent cationic metal organic framework for highly sensitive and selective sensing of chromate anions in natural water systems. *ACS Appl. Mater. Interfaces* **2017**, *9*, 16448−16457.
(22) Zhu, L.; Xiao, C.; Dai, X.; Li, J.; Gui, D.; Sheng, D.; Chen, L.; Zhou, R.; Chai, Z.; Albrecht-Schmitt, T. E.; Wang, S. Exceptional perrhenate/pertechnetate uptake and subsequent immobilization by a low-dimensional cationic coordination polymer: overcoming the hofmeister bias selectivity. *Environ. Sci. Technol. Lett.* **2017**, *4*, 316−322.
(23) Sheng, D.; Zhu, L.; Xu, C.; Xiao, C.; Wang, Y.; Wang, Y.; Chen, L.; Diwu, J.; Chen, J.; Chai, Z.; Albrecht-Schmitt, T. E.; Wang, S. Efficient and selective uptake of TcO_4^- by a cationic metal-organic framework material with open Ag^+ sites. *Environ. Sci. Technol.* **2017**, *51* (6), 3471−3479.
(24) Zhu, L.; Sheng, D.; Xu, C.; Dai, X.; Silver, M. A.; Li, J.; Li, P.; Wang, Y.; Wang, Y.; Chen, L.; Xiao, C.; Chen, J.; Zhou, R.; Zhang, C.; Farha, O. K.; Chai, Z.; Albrecht-Schmitt, T. E.; Wang, S. Identifying the recognition site for selective trapping of $^{99}TcO_4^-$ in a hydrolytically stable and radiation resistant cationic metal-organic framework. *J. Am. Chem. Soc.* **2017**, *139* (42), 14873−14876.
(25) Sheng, D.; Zhu, L.; Dai, X.; Xu, C.; Li, P.; Pearce, C. I.; Xiao, C.; Chen, J.; Zhou, R.; Duan, T.; Farha, O. K.; Chai, Z.; Wang, S. Successful decontamination of $^{99}TcO_4^-$ in groundwater at legacy nuclear sites by a cationic metal-organic framework with hydrophobic pockets. *Angew. Chem., Int. Ed.* **2019**, *58*, 4968−4972.
(26) Banerjee, D.; Xu, W.; Nie, Z.; Johnson, L. E. V.; Coghlan, C.; Sushko, M. L.; Kim, D.; Schweiger, M. J.; Kruger, A. A.; Doonan, C. J.; Thallapally, P. K. Zirconium-based metal-organic framework for removal of perrhenate from water. *Inorg. Chem.* **2016**, *55* (17), 8241−8243.
(27) Banerjee, D.; Elsaidi, S. K.; Aguila, B.; Li, B.; Kim, D.; Schweiger, M. J.; Kruger, A. A.; Doonan, C. J.; Ma, S.; Thallapally, P. K. Removal of pertechnetate-related oxyanions from solution using functionalized hierarchical porous frameworks. *Chem. - Eur. J.* **2016**, *22* (49), 17581−17584.
(28) Li, J.; Dai, X.; Zhu, L.; Xu, C.; Zhang, D.; Silver, M. A.; Li, P.; Chen, L.; Li, Y.; Zuo, D.; Zhang, H.; Xiao, C.; Chen, J.; Diwu, J.; Farha, O. K.; Albrecht-Schmitt, T. E.; Chai, Z.; Wang, Shuao. $^{99}TcO_4^-$ remediation by a cationic polymeric network. *Nat. Commun.* **2018**, *9*, 3007.
(29) Katayev, E. A.; Boev, N. V.; Khrustalev, V. N.; Ustynyuk, Y. A.; Tananaev, I. G.; Sessler, J. L. Bipyrrole-and dipyrromethane-based amido-imine hybrid macrocycles. New receptors for oxoanions. *J. Org. Chem.* **2007**, *72* (8), 2886−2896.
(30) Pierce, E. M.; Lilova, K.; Missimer, D. M.; Lukens, W. W.; Wu, L.; Fitts, J.; Rawn, C.; Huq, A.; Leonard, D. N.; Eskelsen, J. R.; Woodfield, B. F.; Jantzen, C. M.; Navrotsky, A. Structure and thermochemistry of perrhenate sodalite and mixed guest perrhenate/pertechnetate sodalite. *Environ. Sci. Technol.* **2017**, *51* (2), 997−1006.
(31) Jurisson, S. S.; Lydon, J. D. Potential technetium small molecule radiopharmaceuticals. *Chem. Rev.* **1999**, *99* (9), 2205−2218.
(32) Alberto, R.; Bergamaschi, G.; Braband, H.; Fox, T.; Amendola, V. $^{99}TcO_4^-$: selective recognition and trapping in aqueous solution. *Angew. Chem., Int. Ed.* **2012**, *51* (24), 9772−9776.
(33) Ravi, A.; Oshchepkov, A. S.; German, K. E.; Kirakosyan, G. A.; Safonov, A. V.; Khrustalev, V. N.; Kataev, E. A. Finding a receptor design for selective recognition of perrhenate and pertechnetate: hydrogen vs. halogen bonding. *Chem. Commun.* **2018**, *54*, 4826−4829.
(34) Stephan, H.; Berger, R.; Spies, H.; Johannsen, B.; Schmidtchen, F. P. Efficient phase transfer of pertechnetate with bicyclic guanidinium compounds. *J. Radioanal. Nucl. Chem.* **1999**, *242* (2), 399−403.
(35) Glenny, M. W.; Lacombe, M.; Love, J. B.; Blake, A. J.; Lindoy, L. F.; Luckay, R. C.; Gloe, K.; Antonioli, B.; Wilsona, C.; Schröder, M. Design and synthesis of heteroditopic aza-thioether macrocycles for metal extraction. *New J. Chem.* **2006**, *30*, 1755−1767.
(36) Ma, H.; Liu, B.; Li, B.; Zhang, L.; Li, Y. G.; Tan, H. Q.; Zang, H. Y.; Zhu, G. Cationic covalent organic frameworks: a simple platform of anionic exchange for porosity tuning and proton conduction. *J. Am. Chem. Soc.* **2016**, *138* (18), 5897−5903.
(37) Du, Y.; Yang, H.; Whiteley, J. M.; Wan, S.; Jin, Y.; Lee, S. H.; Zhang, W. Ionic covalent organic frameworks with spiroborate linkage. *Angew. Chem.* **2016**, *128* (5), 1769−1773.
(38) Huang, N.; Wang, P.; Addicoat, M. A.; Heine, T.; Jiang, D. Ionic covalent organic frameworks: Design of a charged interface aligned on 1D channel walls and its unusual electrostatic functions. *Angew. Chem., Int. Ed.* **2017**, *56* (18), 4982−4986.
(39) Li, Z.; Li, H.; Guan, X.; Tang, J.; Yusran, Y.; Li, Z.; Xue, M.; Fang, Q.; Yan, Y.; Valtchev, V.; Qiu, S. Three-dimensional ionic covalent organic frameworks for rapid, reversible, and selective ion exchange. *J. Am. Chem. Soc.* **2017**, *139* (49), 17771−17774.
(40) Chen, H.; Tu, H.; Hu, C.; Liu, Y.; Dong, D.; Sun, Y.; Dai, Y.; Wang, S.; Qian, H.; Lin, Z.; Chen, L. Cationic covalent organic framework nanosheets for fast Li-ion conduction. *J. Am. Chem. Soc.* **2018**, *140* (3), 896−899.
(41) Huang, N.; Wang, P.; Jiang, D. Covalent organic frameworks: a materials platform for structural and functional designs. *Nat. Rev. Mater.* **2016**, *1*, 16068.
(42) He, L.; Liu, S.; Chen, L.; Dai, X.; Li, J.; Zhang, M.; Ma, F.; Zhang, C.; Yang, Z.; Zhou, R.; Chai, Z.; Wang, S. Mechanism unravelling for ultrafast and selective $^{99}TcO_4^-$ uptake by a radiation-resistant cationic covalent organic framework: a combined radiological experiment and molecular dynamics simulation study, *Chem. Sci.* **2019**, .

DOI: 10.1021/acs.est.8b06244
Environ. Sci. Technol. 2019, 53, 5212−5220

(43) Mitra, S.; Kandambeth, S.; Biswal, B. P.; Khayum, M. A.; Choudhury, C. K.; Mehta, M.; Kaur, G.; Banerjee, S.; Prabhune, A.; Verma, S.; Roy, S.; Kharul, U. K.; Banerjee, R. Self-exfoliated guanidinium-based ionic covalent organic nanosheets (iCONs). *J. Am. Chem. Soc.* **2016**, *138* (8), 2823−2828.
(44) Kandambeth, S.; Venkatesh, V.; Shinde, D. B.; Kumari, S.; Halder, A.; Verma, S.; Banerjee, R. Self-templated chemically stable hollow spherical covalent organic framework. *Nat. Commun.* **2015**, *6*, 6786.
(45) Baek, K.; Yun, G.; Kim, Y.; Kim, D.; Hota, R.; Hwang, I.; Xu, D.; Ko, Y. H.; Gu, G. H.; Suh, J. H.; Park, C. G.; Sung, B. J.; Kim, K. Free-standing, single-monomer-thick two-dimensional polymers through covalent self-assembly in solution. *J. Am. Chem. Soc.* **2013**, *135* (17), 6523−652.
(46) Zhou, T.-Y.; Lin, F.; Li, Z.-T.; Zhao, X. Single-step solution-phase synthesis of free-standing two dimensional polymers and their evolution into hollow spheres. *Macromolecules* **2013**, *46* (19), 7745−7752.
(47) Qi, X.; Li, L.; Tan, T.; Chen, W.; Smith, J. R. L. Adsorption of 1-butyl-3-methylimidazolium chloride ionic liquid by functional carbon microspheres from hydrothermal carbonization of cellulose. *Environ. Sci. Technol.* **2013**, *47* (6), 2792−2798.
(48) Fei, H.; Bresler, M. R.; Oliver, S. R. J. A new paradigm for anion trapping in high capacity and selectivity: crystal-to-crystal transformation of cationic materials. *J. Am. Chem. Soc.* **2011**, *133* (29), 11110−11113.
(49) Huang, N.; Zhai, L.; Xu, H.; Jiang, D. Stable covalent organic frameworks for exceptional mercury removal from aqueous solutions. *J. Am. Chem. Soc.* **2017**, *139* (6), 2428−2434.
(50) Durant, G. J. Guanidine derivatives acting at histaminergic receptors. *Chem. Soc. Rev.* **1985**, *14*, 375−398.
(51) Custelcean, R.; Moyer, B. A. Anion separation with metal-organic frameworks. *Eur. J. Inorg. Chem.* **2007**, *10*, 1321−1340.
(52) Pearson, R. G. Hard and soft acids and bases. *J. Am. Chem. Soc.* **1963**, *85*, 3533−3539.
(53) Dickson, J.; Harsh, J. B.; Lukens, W. W.; Pierce, E. M. Perrhenate incorporation into binary mixed sodalites: The role of anion size and implications for technetium-99 sequestration. *Chem. Geol.* **2015**, *395*, 138−143.
(54) Rochester, C. H.; Yong, G. H. Infrared study of the adsorption of amines on silica immersed in carbon tetrachloride. *J. Chem. Soc., Faraday Trans. 1* **1980**, *76*, 1158−1165.
(55) Yan, Q. L.; Cohen, A.; Chinnam, A. K.; Petrutik, N.; Shlomovich, A.; Burstein, L.; Gozin, M. A layered 2D triaminoguanidine-glyoxal polymer and its transition metal complexes as novel insensitive energetic nanomaterials. *J. Mater. Chem. A* **2016**, *4*, 18401−18408.
(56) Yan, Q. L.; Cohen, A.; Petrutik, N.; Shlomovich, A.; Burstein, L.; Pang, S. P.; Gozin, M. Highly insensitive and thermostable energetic coordination nanomaterials based on functionalized graphene oxides. *J. Mater. Chem. A* **2016**, *4*, 9941−9948.
(57) Dickson, J. O.; Harsh, J. B.; Flury, M.; Lukens, W. W.; Pierce, E. M. Competitive incorporation of perrhenate and nitrate into sodalite. *Environ. Sci. Technol.* **2014**, *48*, 12851−12857.

DOI: 10.1021/acs.est.8b06244
Environ. Sci. Technol. 2019, 53, 5212−5220